1.11 A MODELING STUDY OF THE FRONTAL CIRCULATIONS ASSOCIATED WITH A HEAVY SNOWBAND IN AN EXTRATROPICAL CYCLONE

Mei Han[1], Mohan K. Ramamurthy[2], Robert M. Rauber, Brian F. Jewett, and Joe A. Grim
Department of Atmospheric Sciences
University of Illinois at Urbana-Champaign, Urbana, IL

1. INTRODUCTION

The northwest quadrant of wintertime extratropical cyclones is commonly associated with heavy snow and blizzard conditions. Radar reflectivity usually reveals banded structure in this region. The precipitation bands are believed to be associated with the trough of warm air aloft, or trowal (Martin, 1998), and the deformation flow associated with cyclones and fronts. A review of the structure, dynamics and associated circulations of upper-level frontal zones was presented by Keyser and Shapiro (1986). Case studies show that a thermally direct circulation associated with upper-level frontogenesis can be attributed to rainband formation (Martin et al., 1992, Lagouvardos et al, 1995). Other dynamic forcing mechanisms, such as conditional symmetric instability, have been extensively studied as well. However, these dynamic mechanisms are believed to occur on different scales. In this paper, frontal circulations will be examined for a heavy snowband in an extratropical cyclone.

On 10-11 December 1997, a cyclone of moderate strength swept through the Ohio valley. A swath of heavy snowfall, with 15-30 cm accumulations, was produced by a mesoscale precipitation band northwest of the cyclone center in southern Michigan and northern Indiana. The structure of this band will be presented in a companion paper in this conference (Grim et. al., 2003). In this paper, a simulation of this band with the NCAR-PSU MM5 model will be employed to analyze the frontal structure, dynamic forcing, and associated secondary circulations which account for the rising motion that produced the wide band and the narrow bands associated heavy snowfall.

2. MM5 SIMULATIONS

The NCAR-PSU MM5 Version 3 model was used to investigate the banded precipitation structure and its environment. The model grid consists of an outer 81-km domain, a middle 27-km domain, and an inner 9-km domain (Fig. 1). 46 vertical layers were employed. The simulation was initialized at 0000 UTC 10 December 1997 and lasted for 24 hours. NCEP Global Data Assimilation System analyses were used for initial and boundary conditions on the outermost domain, while NCEP Rapid Update Cycle fields provided initial condition data on the inner two grids. The simple ice (Dudhia) microphysics, the Grell cumulus parameterization, the Blackadar boundary layer, and a multi-layer soil model were employed.

Figure 1: Geographical locations of the three grids used in the numerical simulation described in the text.

The MM5 24-h accumulated precipitation, sea level pressure (SLP), geopotential height at 500 mb, and jet stream location and intensity at 300 mb verified well against observations. Wide and narrow snowbands were observed in the radar reflectivity field. These were captured in simulated rainwater fields in domain 2 (Fig 2) and domain 3. Model simulations with different resolution were applied to explore the forcing mechanisms for the wide and narrow bands.

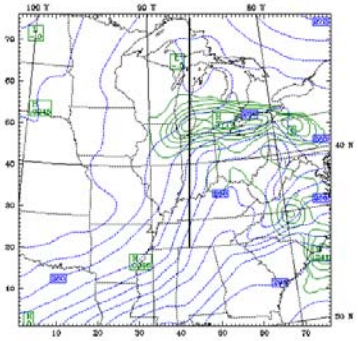

Figure 2: 900 mb rainwater mixing ratio (0.05g/kg , green solid line) and θ (2 K, blue dashed line) in domain 2 at 1600 UTC 10 Dec 1997. Black line: cross section.

3. QG AND FRONTAL FORCING MECHANISMS FOR THE WIDE SNOWBAND

Smoothed MM5 output, with a cutoff wavelength of 108 km, was used to investigate the formation of the wide region of snowfall in the vicinity of the trowal.

1. Corresponding Author Address: Mei Han, University of Illinois, Dept. Atmos. Sci., 105 S. Gregory St. Urbana. IL. 61801. Email: han@atmos.uiuc.edu
2. Current Affiliation: Unidata/UCAR

Fig. 3a shows the quasigeostrophic (QG) vertical motion diagnosed using the omega equation at 700 mb at 1600 UTC. Due to QG forcing, a large area of rising motion in the Midwest was ahead of the synoptic trough and sinking motion followed it. This QG part of rising motion was quite uniform and weak in southern Michigan where the snowband was located.

In contrast with the QG vertical motion, the simulated total vertical motion exhibited significant local enhancement. A banded ascent region was clearly manifested in the non-QG rising motion field generated by subtracting the QG vertical motion from the total vertical motion. This region of non-QG rising motion was most prominent at 700 mb after 1400 UTC. Fig. 3b shows the non-QG vertical motion at 700 mb at 1600 UTC. This banded ascent region matches very well with the snowband illustrated by the rainwater mixing ratio field (Fig. 2).

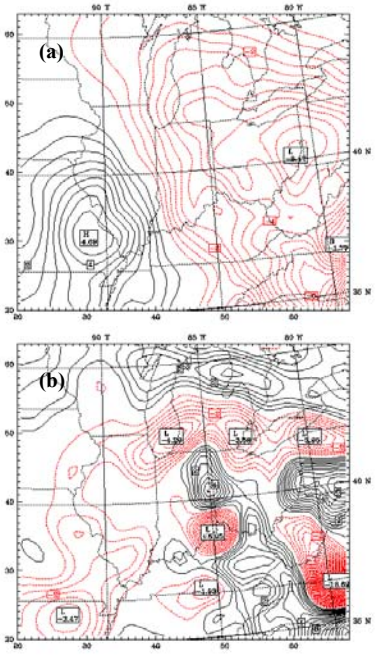

Figure 3: 700 mb vertical motion (dPa/s) at 1600 UTC 10 Dec 1997. (a) QG vertical motion. (b) Non-QG vertical motion. Red: rising motion, black: sinking motion.

To analyze the Non-QG forcing mechanism, a two-dimensional frontogenesis function was examined. In a cross section (see Fig. 2), partitions of the frontogenesis function, due to confluence, horizontal shear, vertical tilting, and diabatic processes, were analyzed (Fig. 4). The confluence term (Fig. 4a) was not very strong, and horizontal shear (Fig. 4b) dominated over confluence due to the strong cyclonic vortex near the front. Fig. 4c shows that the vertical tilting term was very strong and complicated. An axis of maximum vertical motion (See bold vectors in Fig. 4) was located along the center of the snowband. As a result of the vertical tilting term, this vertical motion contributed to frontogenesis to the south of the axis and frontolysis to the north of it at levels below 650 mb, and the opposite couplet with frontolysis to the south and frontogenesis to

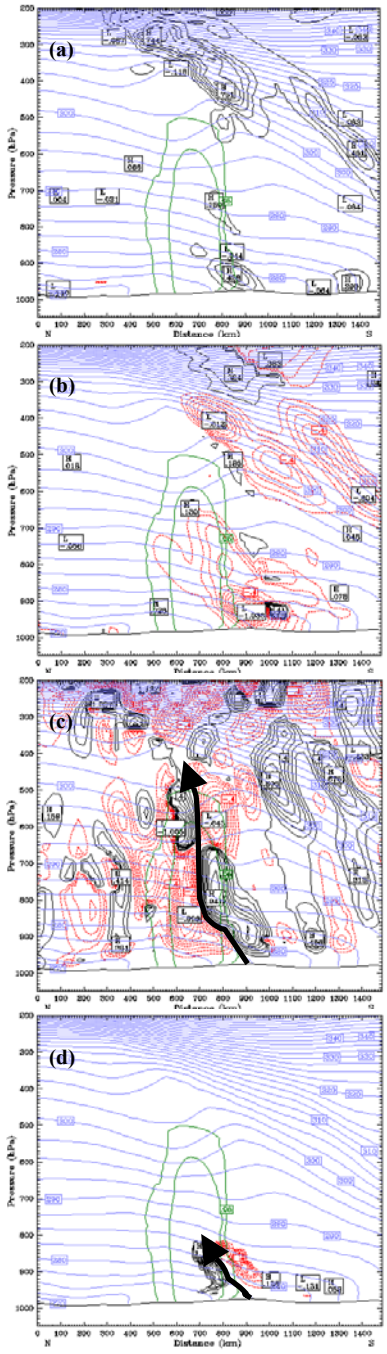

Figure 4: 2 dimensional frontogenesis function (0.1 K/(100 km h)) at 1600 UTC 10 Dec 1997, see Fig. 2 for the location of cross section. (a) Confluence (b) Shearing (c) Tilting (d) Diabatic heating. Frontogenesis is in black and frontolysis is in red. Blue: θ, green: rainwater field (0.05, and 0.15g/kg). Bold vectors: axis of maximum rising motion.

the north in the middle levels in the vicinity of the trowal. Diabatic heating was diagnosed by assessing condensational heating where saturated ascent occurred. This diabatic heating played a moderate role over a small region, where moisture was advected upward and condensed upon reaching the lifting

condensation level (LCL) (Fig. 4d). The maximum condensational heating associated with the maximum rising motion explained the accompanying frontogenesis and frontolysis couplet found in the layer below 800 mb .

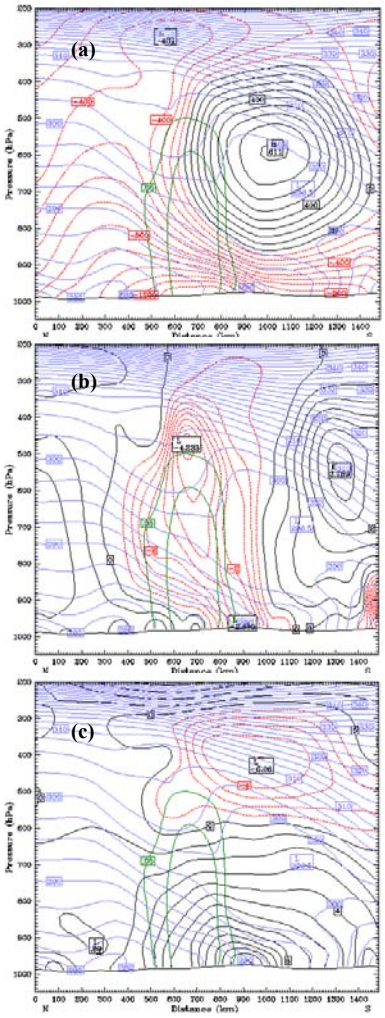

Figure 5: Sawyer-Eliassen streamfunction (a, 100 m hPa/s), derived vertical motion (b, 0.5 dPa/s) and ageostrophic wind (c, 1 m/s) in domain 2 at 1600 UTC 10 Dec 1997 (same cross section as Fig. 4). Positive values are in black and negatives in red. Red means northerly ageostrophic wind in c. Blue: θ_e, green: rainwater (0.05, and 0.15 g/kg).

The ageostrophic secondary circulations were investigated by solving the Sawyer-Eliassen (SE) equation under the geostrophic momentum approximation (GM). Two forcing terms, the geostrophic horizontal stretching deformation (i.e., the confluence term in the frontogenesis discussion) and geostrophic horizontal shearing deformation, were included. No vertical tilting effect was present in the GM SE equation. The effect of moisture on static stability was included.

The SE equation was first solved in a cross section in the western portion of the snowband, i.e., the same cross section for the frontogenesis analysis (See Fig. 2). The SE streamfunction derived from the total horizontal deformation, and the derived omega and ageostrophic wind are shown in Fig. 5. Green lines depict the outline of the rainwater field. This figure exhibits an indirect circulation: its rising branch collocated with the snowband and sinking branch south of it. Partitions of the streamfunction were also examined (not shown), which indicated that the stretching deformation led to frontogenesis and induced a direct circulation, while the shearing deformation resulted in frontolysis and produced an indirect circulation. However, the shearing deformation dominated stretching deformation, and the total ageostrophic circulation was an indirect circulation.

Another cross-section located near the eastern end of the snowband was chosen to examine the along-front variation of the ageostrophic circulation (figures not included). It revealed that the stretching term dominated the shearing term, so that frontogenesis was the net effect. The rising branch of the resultant direct circulation contributed to the formation of the eastern end of the snowband.

The horizontal wind and potential temperature were also examined, which showed consistency between the deformation flow and the frontogenesis/frontolysis analysis performed in the cross sections above. A cyclonic vortex was located near the border of Illinois and Indiana, and extended from surface to 500 mb. South of the vortex, a 500 mb jet streak extended from WSW to ENE. The west portion of the snowband was close to the vortex center and north of the jet streak. Both contributed to the shearing deformation which dominated the stretching deformation and led to frontolysis. The east end of the band was away from the vortex and the jet streak. Confluence associated with the warm front at lower levels and the exit region of the jet streak at higher levels dominated and produced frontogenesis leading to a direct circulation.

As discussed in the previous section, the tilting process dominated the other three mechanisms in the 2-D frontogenesis function. Unfortunately, the SE equation under the GM approximations does not incorporate tilting. However, we can view its response from the individual circulations associated with every cell of frontogenesis/frontolysis. In the snowband region, two opposite frontogenetic/frontolytic couplets were analyzed in the trowal and below (Fig. 4c), which were caused by the maximum rising motion at the center of the precipitation band. The sinking branches of the secondary circulations associated with the four cells of frontogenesis/frontolysis were all located in the center of the band. The result (sinking motion) is opposite to the primary forcing (rising motion), an example of "LeChatelier's Principle".

4. DYNAMIC FORCING FOR THE NARROW EMBEDDED BAND

Domain 3 (9 km grid spacing) data revealed narrow bands embedded in the wide band. Fig. 6 shows the potential temperature and the rainwater fields along a cross section along the border of Illinois and Indiana

at 1200 UTC 10 December 1997. It was evident from the animation of these fields that wave trains were propagating northward between the surface front and tropopause. The snowbands appear to be associated with the waves, because (1) the scales of the precipitation bands and the waves were comparable, and (2) the waves appeared to help organize the bands.

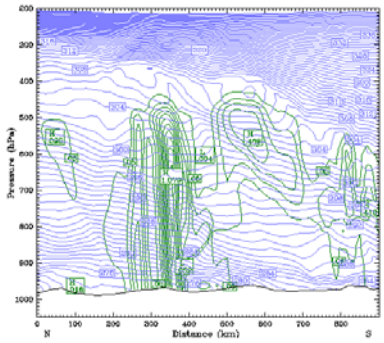

Figure 6: θ cross section(blue: 1 K) and rainwater (green: 0.001, and every 0.1 g/kg) at 1200 UTC.

We investigated the evolution of the potential temperature and rainwater fields in order to figure out whether the precipitation bands induced the waves or the other way around. Fig.7 shows the equivalent potential temperature cross section at 54 minutes and 120 minutes from model initial time (same location as in Fig. 6). The two vectors stands for the differential wind suggested by dropsonde observations and the model simulation. These vectors indicate differential warm advection from south. Because of differential warm advection, the isentropes tilted from slantwise to vertical from panel a to b. The precipitation then initiated (figure not shown). This suggests that the differential warm advection destabilized the atmosphere and led to the formation of the wide band. The animation also suggested that evaporative cooling associated with the precipitation induced waves at later time. The waves propagated, modified the atmosphere, and helped to organize precipitation into banded structure later in the simulation.

5. CONCLUSION AND DISCUSSION

A detailed analysis of the forcing for vertical motion within the snowband was presented through diagnosis of the model output using the geostrophic momentum form of the Sawyer-Eliassen equation. Ageostrophic circulations associated with both frontogenetic and frontolytic forcing in the vicinity of the warm front and the trough of warm air aloft were shown to have led to the persistent band of rising motion that produced the heavy snow. The effects of the shearing and stretching deformation were discussed. The analysis showed that the importance of these terms varied along the length of the band, i.e. along the length of the warm front, with shearing deformation dominating the western portion of the band on the north side of the cyclone vortex center and stretching deformation dominating the eastern end of the band that was well east of the cyclone center. The rising branches of the secondary circulation contributed to the formation of the wide snowband, no matter whether frontogenesis or frontolysis occurred.

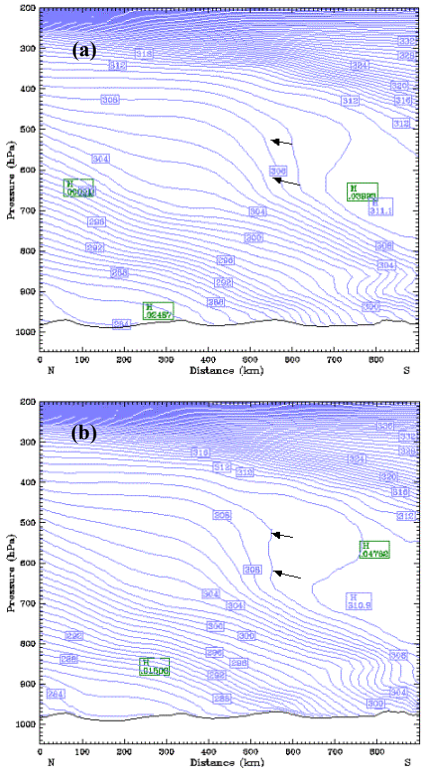

Figure 7: θ_e cross section (blue: 1 K) and rainwater (green) at 54 minutes (a) and 120 minutes (b) .

For the narrow bands, our preliminary conclusion is that differential warm advection destabilized the atmosphere and triggered the initial precipitation that in turn induced the waves through evaporative cooling. These waves modified the atmosphere and organized the precipitation into banded structure. However, the waves need to be characterized in more detail and the modification processes need further investigation. Therefore, we plan to do a 4-grid simulation with 3 km grid spacing in the innermost domain, which would give us more detailed evidence about wave activities and narrow snowbands.

ACKNOWLEDGEMENTS

This work was funded by the NSF under grants NSF ATM 9708170 and NSF 0004274

REFERENCES

Keyser, D. and Shapiro, M. A., 1986: *Mon. Wea. Rev.*, **114,** 452-499.

Lagouvardos, K. and V. Kotroni, 1995: *Mon. Wea. Rev.*, **123**, 1197-1206.

Martin, J. E. et al., 1992: *J. Atmos. Sci.*, **49**, 1293-1303

Martin, J. E., 1998: *Mon. Wea. Rev.*, **126**, 303-328.